Iranian Journal of Physics Research, Vol. 18, No. 3, 2018

The electrical transport properties in ZnO bulk, ZnMgO/ZnO and ZnMgO/ZnO/ZnMgO heterostructures

M Amirabbasi and I Abdolhosseini Sarsari
Department of Physics, Isfahan University of Technology, Isfahan, Iran

E-mail: m.amirabbasi@ph.iut.ac.ir

(Received 13 January 2017 ; in final form 17 December 2017)

Abstract
In this paper, the reported experimental data related to electrical transport properties in bulk ZnO, ZnMgO/ZnO and ZnMgO/ZnO/ZnMgO single and double heterostructures were analyzed quantitavely and the most important scattering parameters on controlling electron concentration and electron mobility were obtained. Treatment of intrinsic mechanisms included polar-optical phonon scattering, piezoelectric scattering and acoustic deformation potential scattering. For extrinsic mechanisms, ionized impurity, dislocation scattering and strain induced fields were considered. For the bulk ZnO, the reported experimental data were corrected for removing the effects of a degenerate layer at the ZnO/sapphire interface via a two – layer Hall – effect model. Also, donor density, acceptor density and donor activation energy were determined via the charge balance equation. This sample exhibited hopping conduction below 50K and dislocation scattering controled electron mobility closely. Obtained results indicated that the enhancement of electron mobility in the double sample, as compared with single one, could be attributed to the reduction of dislocation density, two-dimensional impurity density in the potential well due to background impurities, and/or interface charge and strain induced fields which can be related to the better electron confinement in the channel and enhancement in the sheet carrier concentration of 2DEG in this sample.

Keywords: ZnMgO/ZnO/ZnMgO, ZnO/sapphire interface, heterostructures, scattering mechanisms

1. Introduction

ZnO has received substantial interest in the research community due to its wide band gap (3.4 eV) [1], high breakdown voltage, generation lower noise, high temperature power, and sustained large electrical field [2-5]. ZnOs are used in a variety of optical and optoelectronic applications such as UV light – emitting diodes [6,7], transparent transistors [8], UV detectors [9], and UV laser diodes [10,11]. In the Bulk ZnO, the mobility is decreased at low and high temperatures due to dislocation scattering, ionized impurity and lattice vibrations, respectively. Undoped ZnO with a wurtzite structure is naturally an n-type semiconductor due to the presence of intrinsic defects such as Zn interstial and O vacancy [5]. To make high quality P-type ZnO, knowing the native defects in an undoped ZnO via Hall effect measurements is essential. To obtain high mobility, especially at low temperatures, ZnMgO/ZnO heterostructures [12,13] in which electrons have a two-dimensional space are used. Consequently, a two-dimensional electron gas (2DEG) is formed at the interface due to the internal electric field. Since carrier confinement can be influence electron mobility, ZnMgO/ZnO/ZnMgO double quantum is well fabricated recently [14,15]. The ability to fabricate a ZnMgO-hetero structures makes it possible to fabricate ZnMgO – high electron mobility transistors (HEMT) [16] which have received more attention recently [17,19]. Transport properties such as carrier mobility (μ) and carrier concentration (n) are crucially important because operation of all these devices critically depends on the current transport.

In this paper, the reported experimental data related to electrical transport properties in the bulk ZnO, ZnMgO/ZnO and ZnMgO/ZnO/ZnMgO with single and double heterostructures were analyzed quantitavely, as reported by J. Ye *et al.* [20]. The bulk ZnO, $Zn_{0.82}Mg_{0.18}O$ (75 nm) /ZnO single (sample A) and $Zn_{0.8}Mg_{0.2}O$ (60 nm)/ZnO (30 nm)/graded-$Zn_{0.85}Mg_{0.15}O$ (90 nm) double (sample B) heterostructures were grown

Table 1. ZnO material parameters used in the calculation.

Material parameters	Values
Density of the crystal (ρ) [23]	6.1×10^3 (kgm^{-3})
Deformation potential energy (E_l) [24]	3.5 (eV)
High-frequency dielectric constant (ε_∞) [22]	$3.72\varepsilon_0$ (Fm^{-1})
Static dielectric constant (ε_s) [22]	$8.12\ \varepsilon_0$ (Fm^{-1})
Effective mass (m^*) [22]	$0.3m_0$ (kg)
ZnO lattice constant (a_0) [17]	0.521 (nm)
Piezoelectric constant (h_{pz})[23]	1.10 (cm^{-2})
Electron mass (m)	9.1096×10^{-31}(kg)
Sound velocity (s)[23]	6.59×10^3 (ms^{-1})
MgO lattice constant (a_l) [17]	0.421 (nm)
Longitudinal acoustic phonons velocity (u_l) [17]	6.4×10^3 (ms^{-1})
Transverse acoustic phonons velocity (u_s) [17]	3.5×10^3 (ms^{-1})

on sapphire by using the metal-organic vapor phase epitaxy technique [20]. The experimental details are given in ref. [20]. Also, the sheet carrier concentrations (n_s) of 2DEG in the samples A and B have been reported to be 1.48×10^{12} and 1.16×10^{14} cm^{-2}, respectively [20]. Since the dimension of our system is further than the dimension of mesoscopic systems, we did not consider quantum transport; also, electron – electron correlation effects for 3d orbital (for Zn atom), which play an important role in quantum transport, were neglected in this material.

2. Theory of electrical properties

2.1 . Charge balance equation

I have used the charge balance equation for the carrier concentration data in which semiconductor is assumed to be the n-type non-degenerate [21]:

$$n + N_a = \sum_i \frac{N_{di}}{1 + \frac{n}{\phi_i}}, \tag{1}$$

where

$$\phi_i = (g_{0i} / g_{1i}) N_c \exp(\alpha_i / k_B) \exp(-E_{d0i} / k_B T), \tag{2}$$

$$N_c = 2(2\pi m^* k_B / h^2)^{3/2}, \tag{3}$$

where N_a is the acceptor density, N_d is the donor density, g_{0i} (g_{1i}) is the unoccupied (occupied) state degeneracy of the donor i, and α is the temperature coefficient defined by $E_{di} = E_{d0i} - \alpha_i T$, in which E_d, E_{d0} refer to the activation energy of the donor electrons at T and zero temperature, respectively [5] (α is assumed to be zero [22]). It should be noted that N_a, N_d and Ed are considered as the fitting parameters.

2.2 Theory of scattering mechanisms in Bulk semiconductors

Here, the mobility limit due to each individual scattering process is calculated independently, using their corresponding analytical expressions (μ_i). The total mobility can be calculated from the scattering – limiting motilities by using the Matthiessen's rule ($\frac{1}{\mu} = \sum_i \frac{1}{\mu_i}$).

The material parameters used in the calculations are listed in table 1.

2. 2. 1. Intrinsic scattering mechanisms

(I) The mobility (μ_{ac}) of the bulk electron scattered from acoustic deformation potential scattering is given by [25]:

$$\mu_{ac}(T) = \frac{2(2\pi)^{1/2} \rho s^2 \hbar^4 e}{3E_l^2 (m^*)^{5/2} (k_B T)^{3/2}}, \tag{4}$$

where El, ρ and s are deformation potential energy, density of the crystal and sound velocity, respectively.

(II) The mobility (μ_{pz}) limited by piezoelectric scattering is expressed as [25]:

$$\mu_{pz}(T) = \frac{16(2\pi)^{1/2} \rho s^2 \hbar^2 e}{3(e h_{pz} / \varepsilon_s \varepsilon_0)^2 (m^*)^{3/2} (k_B T)^{1/2}}, \tag{5}$$

where h_{pz} is the piezoelectric constant in ZnO.

(III) The mobility (μ_{pop}) caused by the polar optical phonon scattering, which controls carrier mobility at the high temperature, can be calculated using [26]:

$$\mu_{pop}(T) = 0.199(T/300)^{1/2} (e/e^*)^2 (m/m^*)^{3/2} (10^{22} M)(10^{23} V_a)(10^{-13}\omega)(\exp(\hbar\omega / k_B T) - 1) G(\hbar\omega / k_B T), \tag{6}$$

Here, ω, $e^* = \sqrt{M V_a \omega \varepsilon_0 (1/\varepsilon_\infty - 1/\varepsilon_s)}$, V_a and M are the polar phonon frequency, Callen's effective ionic charge, volume for a Zn and O ion pair and reduced ionic mass, respectively.

2. 2. 2. Extrinsic scattering mechanisms

(I) The mobility (μ_{Im}) determined by the Ionized impurity scattering is given by [27, 28]:

$$\mu_{\mathrm{Im}}(T) = \frac{128(2\pi)^{1/2} (\varepsilon_s \varepsilon_0)^2 (k_B T)^{3/2}}{e^3 (m^*)^{1/2} (n + 2N_a)} \left[\ln(1+b) - \frac{b}{b+1} \right]^{-1}, \tag{7}$$

where N_a is the acceptor density which is obtained from equation (1) as the fitting parameter.

(II) The mobility (μ_{cd}) caused by the crystalline defects (domain boundaries and strain induced fields) scattering can be obtained from [28]:

$$\mu_{cd}(T) = C / T^{1.5}, \tag{8}$$

Here, C is attributed to the strained induced fields and domain boundaries.

(III) The mobility limited (μ_{disl}) by dislocation scattering that controls carrier mobility at low temperatureis expressed as [29]:

$$\mu_{disl}(T)=\frac{30(2\pi)^{1/2}(\varepsilon_0\varepsilon_s)^2a^2(k_BT)^{3/2}}{N_{disl}e^3f^2\lambda_D(m^*)^{1/2}}, \quad (9)$$

where N_{disl}, f (=1), a and $\lambda_D=\left(\frac{\varepsilon_s\varepsilon_0k_BT}{e^2n}\right)^{1/2}$ is dislocation density, occupancy rate and distance between acceptor centers, respectively.

2.3. Two – layer Hall – effect model

Due to the lattice mismatch between the semiconductor layer and the substrate, a narrow area with high dislocation density (degenerated layer) was formed in semiconductor layer/ substrate interface, with crucial effects on the electrical properties (carrier concentration and mobility) of the semiconductor, especially at low temperatures. We can use the two-layer Hall Effect – model to correct the carrier concentration and the mobility experimental data [30]:

$$n_1=\frac{(\mu_Hn_H-\mu_2n_2)^2}{\mu_H{}^2n_H-\mu_2{}^2n_2}, \quad (10)$$

$$\mu_1=\frac{\mu_H{}^2n_H-\mu_2{}^2n_2}{\mu_Hn_H-\mu_2n_2}, \quad (11)$$

where μ_H and n_H are the experimental mobility and carrier concentration, μ_2 and n_2 are the mobility and carrier concentration in the degenerated layer, and μ_1 and n_1 are the corrected data.

2.4. Theory of scattering mechanisms in 2DEG

Different scattering mechanisms have been considered to model the 2DEG mobility by using the Matthiessen's rule. The analytical expressions of scattering mechanisms for 2DEG mobility are briefly summarized below and the relevant material parameters are listed in table 1.

2.4.1. Intrinsic scattering mechanisms

(I) The polar optical phonon scattering is expressed as [31, 32]:

$$\mu_{pop}(T)=\frac{4\pi\varepsilon_0\varepsilon_p\hbar^2}{e\omega(m^*)^2L}\left[\exp(\hbar\omega/k_BT)-1\right] \quad (12)$$

where L ($=2(\frac{n_s}{10^{12}\,\mathrm{cm}^{-2}})^{-1/3}\times 55$ Å) [33] is the width of the quantum well, n_s is 2DEG sheet carrier density, and

$$1/\varepsilon_p=1/\varepsilon_\infty-1/\varepsilon_s \quad (13)$$

(II) The acoustic deformation potential scattering is given by [34]:

$$\mu_{ac}(T)=\frac{e\hbar^3\rho u_l{}^2L}{m^{*2}E_l{}^2k_BT} \quad (14)$$

Here, u_l is the longitudinal acoustic phonon velocity.

(III) In strongly polar materials, the most powerful interaction with acoustic phonons at low energies is via the piezoelectric effect. The piezoelectric scattering can be obtained from [35]:

$$\mu_{pz}(T)=\frac{\pi k_fE_l{}^2}{Le^2h_{14}{}^2}\left[\frac{9}{32}+\frac{13}{32}(\frac{u_l}{u_t})^2\frac{I_A(\gamma_t)}{I_A(\gamma_l)}\right]^{-1}\mu_{dp}, \quad (15)$$

where k_f (= $(2\pi n_s)^{1/2}$) is the wave vector on the Fermi surface, h_{14} is the piezoelectric constant, u_t is the transverse acoustic phonon velocity, and

$$I_A(\gamma_t)=\left[\left(\frac{4\gamma_t}{3\pi}\right)^2+1\right]^{1/2}, \quad (16)$$

$$I_A(\gamma_l)=\left[\left(\frac{4\gamma_l}{3\pi}\right)^2+1\right]^{1/2}, \quad (17)$$

$$\gamma_t=\frac{2\hbar u_tk_f}{k_BT}, \quad (18)$$

$$\gamma_l=\frac{2\hbar u_lk_f}{k_BT}, \quad (19)$$

2.4.2. Extrinsic scattering mechanisms

(I) In heterostructures with 2DEG, although free electrons are separated from the ionized donors, they can still be scattered from them. The mobility is caused by ionized impurity scattering due to remote donors scattering [33]:

$$\mu_{\mathrm{remote}}(T)=\frac{64\pi\hbar^3k_f{}^3\varepsilon_0{}^2\varepsilon_s{}^2s_0{}^2}{e^3(m^*)^2N_d}\left(\frac{1}{L_0{}^2}-\frac{1}{LM_0{}^2}\right)^{-1}, \quad (20)$$

where

$$L_0=d_0+L/2, \quad (21)$$

$$LM_0=L_0+d_1, \quad (22)$$

Here, d_0 is the width of the spacer layer and d_1 is the width of the depletion layer ($\approx n_s/N_d$, with N_d as the donor density in the barrier), and S_0 ($=\frac{e^2m^*}{2\pi\varepsilon_0\varepsilon_s\hbar^2}$) is the the screening constant [36].

(II) In ZnMgO/ZnO heterostructures, 2DEG is formed on the ZnO side of the ZnMgO heterointerface and hence, background impurity scatters free carriers, as well as the interface charge. Ionized impurity scattering due to the interface charges can be calculated from [37, 38]:

$$\mu_{bi}=\frac{4\pi\varepsilon_0{}^2\varepsilon_s{}^2\hbar^3k_f{}^3}{e^3(m^*)^2N_{bi}I_B}, \quad (23)$$

where N_{bi} is the 2D impurity density in the potential well due to the background impurities and/or interface charge and

$$I_B=\int_0^\pi\frac{\sin(\varphi)}{\left[2\sin(\varphi)+\frac{S_0}{k_f}\right]^2}d\varphi \quad (24)$$

(III) The dislocation scattering is expressed as [39-40]:

$$\mu_{disl}=\frac{4\pi\varepsilon_0{}^2\varepsilon_s{}^2\hbar^3k_f{}^4c^2}{e^3(m^*)^2N_{\mathrm{disl}}I_t} \quad (25)$$

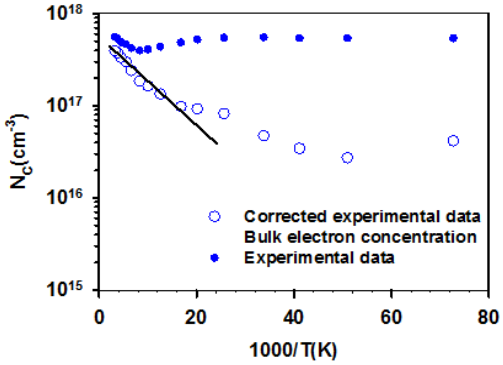

Figure 1. (color onlin) The experimental and bulk (corrected) electron concentration versus temperature (the solid curve shows the result fitted to the corrected data).

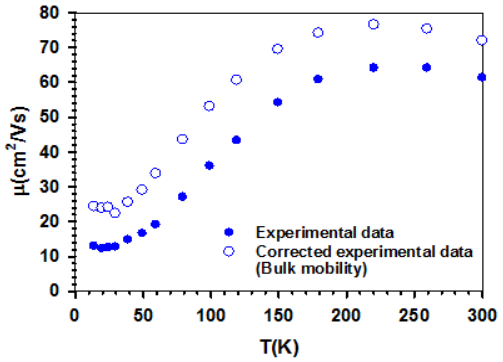

Figure 2. (color onlin) The experimental and bulk (corrected) electron mobility versus temperature.

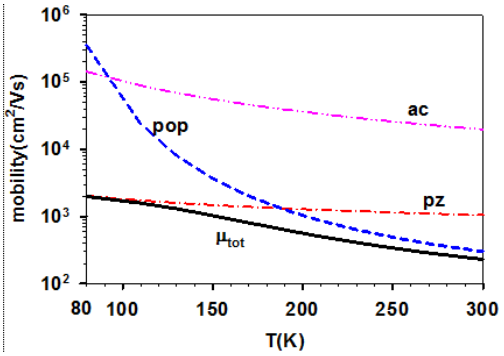

Figure 3. (color onlin) Total mobility (solid curve) of the hypothetically pure ZnO, as calculated using the Matthiesen's rule. The mobility limits due to the lattice scattering mechanisms are displayed in the dashed curves.

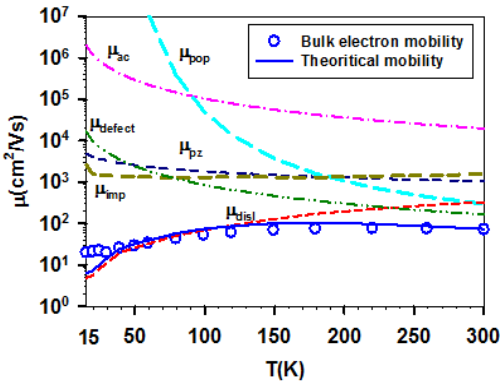

Figure 4. (color onlin) The bulk electron mobility fittings for the n-type ZnO sample.

where N_{disl} is the charge dislocation density, c is the lattice constant of $In_{1-x}Al_xN$ [$=xa_l(AlN)+(1-x)c(InN)$ as suggested by Vegard's law], ξ is a dimensional parameter: $\xi=2kF/qT_F$, $qT_F=2/a_B$ is the 2D Thomas-Fermi wave vector, where $a_B = \varepsilon_s\varepsilon_0h^2/\pi e^2m^*$ is the effective Bohr radius in the material and

$$I_t = 1/2\xi^2 \int_0^1 \frac{1}{(1+\xi^2u^2)\sqrt{1-u^2}} d\varphi, \qquad (26)$$

3. Results and discussion

3.1. Bulk mode

The experimental temperature – dependent electron concentration of the ZnO is shown in figure 1. The experimental electron concentration was decreased as the temperature was reduced from 300 to 80 K, which was a carrier freeze – out process; then it was increased slightly when temperature was decreased further. As result, due to the lattice mismatch between ZnO and sapphire, a two-dimensional parallel conduction layer (degenerate layer) was formed at the ZnO/sapphire interface, which was temperature-independent. To investigate the electrical transport properties of the bulk layer, the electron concentration and the electron mobility of the degenerate layer should be removed via a two – layer Hall – effect model (See Eq. 10-11). The corrected data are shown in Figure 1 and Figure 2.

As it is clear from Figure 1 and Figure 2, by removing the effects of the degenerate layer, the bulk electron concentration was reduced (5×10^{17} to 4.1×10^{16} cm^{-3} at 15 K and 5.22×10^{17} to 3.9×10^{17} cm^{-3} at 300K) and the bulk electron mobility was increased (15 to 20 $cm^2V^{-1}s^{-1}$ at 15K and 60 to 71 $cm^2V^{-1}s^{-1}$ at 300K), as compared to their experimental values. For T< 50 K, the slight bulk electron concentration decrease indicated the hopping conduction; then the good fitting between the bulk data and theoretical curves was not obtained . Temperature – dependent bulk electron concentration was fitted by the charge balance equation (See eq. (1)). The obtained fitting values are listed in table 1. The obtained activation energy of the residual donor was in a reasonable agreement with the reported value [41], confirming the validity of my fitting.

Figure 3 shows the total mobility obtained from the Matthiesen's rule by considering the intrinsic scattering mechanisms. As can be seen in figure 3, in the pure ZnO sample, the total mobility at the room temperature was in order of $10^2(cm^2V^{-1}s^{-1})$.

Figure 4 shows the position of each of the scattering mechanisms for the bulk electron mobility of ZnO. The obtained fitting parameters have been listed in table 1. It should be noted that N_{disl} could be matched with the accuracy of the reported values [42] in this case. According to figure 4:

- At the low and medium temperature range, 15 < T < 240 K, dislocation scattering is dominant.

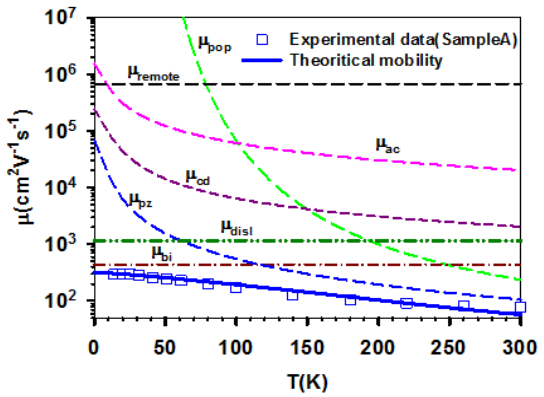

(b)

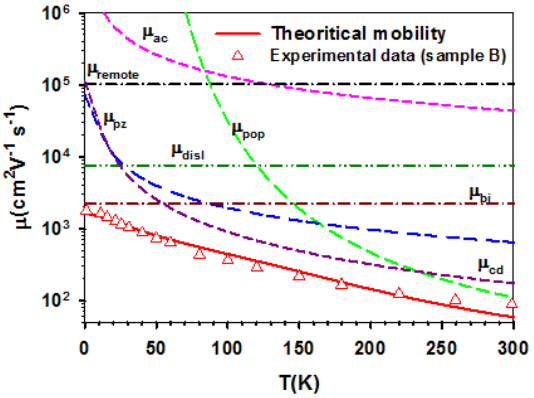

(a)

Figure 5. (color onlin) Experimental and calculated temperature dependence of electron mobility curves for (a) $Zn_{0.82}Mg_{0.18}O$ /ZnO and (b) $Zn_{0.8}Mg_{0.2}O$/ZnO/graded-$Zn_{0.85}Mg_{0.15}O$.

Table 2. The value of the calculated fitting parameters for ZnO.

Value	Fitting parameters
1×10^{16}	N_a (cm^{-3})
6×10^{17}	N_d (cm^{-3})
25	E_d (meV)
6.5×10^{13}	dislocation density N_{disl} (cm^{-3})
8.5×10^{5}	crystalline defects

- At the high temperature range, 240 <T< 300 K, polar optical phonon scattering controls the bulk electron mobility.

3. 2. 2DEG mobility

With respect to Vegard's law and the band gap value of ZnO (= 3.4 eV) [1] and MgO (= 5.88 eV) [43], the band gap value of $Zn_{0.82}Mg$ 0.18 O/ZnO and Zn0.8Mg0.2O/ZnO/Zn0.85$Mg_{0.15}$O was calculated to be about 3.88 eV and 3.89 eV, respectively; this showed that the band gap of ZnMgO/ZnO was wider than ZnO. So, it should be expected that some conduction electrons in the ZnMgO layer were transferred to the adjacent layer with a smaller band gap (ZnO), which caused an internal field; subsequently, the formation of a triangular quantum well and thus, the formation a thin layer near the interface with a 2DEG behavior were expected.

Figure 5 shows the temperature dependence of the electron mobility and the calculated component mobility of the individual scattering process for $Zn_{0.82}Mg_{0.18}O$ (75 nm) /ZnO single (sample A) and $Zn_{0.8}Mg_{0.2}O$ (60 nm) /ZnO(30 nm)/graded-$Zn_{0.85}Mg_{0.15}O$(90 nm) double (sample B) heterostructures. As can be seen clearly, the electron mobility was increased when temperature was decreased, reaching the maximum value of about 290 $cm^2V^{-1}s^{-1}$ and 1780 $cm^2V^{-1}s^{-1}$ for the samples A and B, respectively. The difference was considerable. A very good consistency was obtained between the temperature dependence of the calculated total mobility data and the experimental results. The fitting parameters have been listed in table 2. The investigated structures included the Mg content x in the barrier layer, changing from 0.18 to 0.2; n_s was increased from about 1.48 $\times 10^{12}$ and 1.16 $\times$ 10^{14} cm^{-2} for the samples A and B, respectively. The dislocation scattering and the ionized impurity scattering due to the interface charges were weakened when n_s was increased, and the screening effect of the electrons on the scattering centers was improved (see table 2). The enhancement of electron mobility in the sample B could be associated with the decrease in N_{disl}, N_{bi} and strain induced fields in this sample (see table 2). Also, better electron confinement in heterostructures played an important role in determining the 2DEG mobility via increasing the screening effect against the ionized impurity and dislocation scattering [44-45].

As a result, the produced electric field via piezoelectric polarization charge at the ZnMgO/ZnO heterointerface and the formation of the conduction band discontinuity at the same interface could lead to better electron confinement, leading to the enhancement of the electron mobility of $Zn_{0.8}Mg_{0.2}O$/ZnO/$Zn_{0.85}Mg_{0.15}O$.
As can be seen from figure 5:

- For the sample A, at the low temperature (T< 110K), ionized impurity scattering due to the interface charges and at high temperature (110<T< 300 K), piezoelectric scattering controlled electron mobility.
- For the sample B, at the low temperature (T< 60 K), ionized impurity scattering due to interface charges scattering, at the medium temperature (60<T< 230 K), crystalline defects, and at the high temperature (T> 230 K), polar optical phonon scattering restricted mobility.

It should be noted that the obtained dislocation density could be matched with the accuracy of the reported values [41], which was in the range 10^9 to 10^{11} cm^{-2}.

4. Conclusion

In this paper, the reported experimental data related to the electrical transport properties of ZnO/sapphire, $Zn_{0.82}Mg_{0.18}O$ (75 nm) /ZnO single (sample A) and $Zn_{0.8}Mg_{0.2}O$ (60 nm)/ZnO (30 nm)/graded-$Zn_{0.85}Mg_{0.15}O$ (90 nm) double (sample B) heterostructures were investigated quantitavely with different Mg concentrations and barrier thicknesses. For the bulk

Tabl 2. The values of the calculated fitting parameters for the heterostructures samples.

Fitting parameters	Sample A	Sample B
Dislocation density N_{disl} (m^{-2})	7×10^{12}	1×10^{15}
2D impurity density in the potential well N_{bi} (m^{-3})	9×10^{23}	4.2×10^{25}
C Parameter	5.5×10^{5}	9×10^{5}

ZnO, the effect of the degenerated layer at the ZnO/sapphire interface on the experimental electron concentration and mobility could be removed by using a two – layer Hall – effect model. The fitting curve of temperature-dependent corrected electron concentration, giving E_d= 25meV, $Na = 1 \times 10^{16}$ cm^{-3} and $N_d = 6 \times 10^{17}$ cm^{-3}. The fitting curves of temperature dependence for the corrected electron mobility showed that dislocation scattering restricted electron mobility approximately in all temperature ranges, which could be due to the large lattice mismatch between ZnO and sapphire. The value of N_{disl} in this sample was obtained to be about 6.5×10^{13} cm^{-2}. For $Zn_{0.82}Mg_{0.18}O$/ZnO single and $Zn_{0.8}Mg_{0.2}O$/ZnO/graded-$Zn_{0.85}Mg_{0.15}O$ double heterostructures, the temperature dependence of 2DEG mobility was determined by taking into account all the major scattering mechanisms. The calculated results for 2DEG mobility indicated that in the ZnMgO/ZnO/ZnMgO heterostructure, dislocation and ionized background impurity were effectively suppressed, which could be related to the enhancement in the sheet carrier concentration of 2DEG and better electron confinement in the channel because of the produced electric field via piezoelectric polarization charge and the formation of the conduction band discontinuity at the heterointerface in this sample.

References

1. J Dai, X Han, Z Wu, Y Fang, H Xiong, Y Tian, C Yu, Q He, and C Chen, *Journal of Electronic Materials* **40**, 4 (2011) 466.
2. L Meng, L Zheng, L Cheng, G Li, L Huang, and Y Gu, *J. Materials Chemistry* **21**, 30 (2011) 11418.
3. K Park and H Hwang, J Seo, and W-S Seo, *Energy* **54** (2013) 139.
4. C Pholnak, S Suwanboon, and C Sirisathitkul, *J. Materials Science*: *Materials in Electronics*, **24** (2013) 12 5014.
5. H Morkoc and U Ozgur, "*Zinc Oxide Fundamentals, Materials and Device Technology*", Wiley-Vch (2009).
6. C Wang, R Boa, K Zhao, T Zhang, and L Dong, *Nano Energy* **14** (2015) 364.
7. H Wang, Y Zhao, C Wu, X Dong, B Zhang, G Wu, Y Ma, and G Du, *J. Luminescence* **158** (2015) 6.
8. J Kwon, Y K Hong, H-J Kwon, Y Park, B Yoo, J Kim, C P Grigoropoulos, M S Oh and S Kim, *Nanotechnology* **26** (2015) 035202.
9. L Guoa, H Zhanga, and D Zhaoa, B Lia, Z Zhanga, M Jianga, and D Shen, *Sensors and Actuators* B: *Chemical* **166-167** (2012) 12.
10. Z F Shi, Y T Zhang, X J Cui, S W Zhuang, B Wu, X W Chu, X Dong, B L Zhang, and G T Dou, *Phys. Chem. Chemical Physics* **17** (2015) 13813.
11. M Szymański, H Teisseyre, and A Kozaneck, *Physica Status Solidi* (a) **211** (2014), 2105.
12. J Bian, X Kou, Z Zhang, Y Zhang, J Sun, F Qin, W Liu, and Y Luo, *Materials Science in Semiconductor Processing* **16** (2013) 1684.
13. L Sang, S Y Yang, G P Liu, G J Zhao, B C Liu, C Y Gu, H Y Wei, X L Liu, Q S Zhu, and Z G Wang, *IEEE Trans. Electron Devices* **60** (2013) 2077.
14. H C Wang, C H Liao, Y L Chueh, C C Lai, L H Chen, and R C C Tesiang, *Optical Materials Express* **2** (2013) 237.
15. P Kuznetsov, V Lusanov, G Yakushcheva, V Jitov, L Zakharov, I Kotelyanskii, and V Kozlovsky, *Physica Status Solidi* C **7** (2010) 1568.
16. P Barquinha, E Fortunato, A Goncalves, A Pimmentel, A Marques, L Pereira, and R A Martins, *Adv. Mater. Forum*. **68** (2006) 514.
17. M Amirabbasi, *Modern Phys. Lett*. B **27** (2013) 1350170.
18. X Ji, Y Zhu, M Chen, L Su, A Chen, X Gui, R Xiang, and Z Tang, *Scientific Reports* **4** (2014) 4185.
19. L Meng, J Zhang, Q Li, and X Hou, *Journal of Nanomaterial* **2015**, 26 (2015) 1. http:// dx.doi. org/ 10.1155/2015/694234.
20. J Ye, S T Lim, M Bosman, S Gu, Y Zheng, H Tan, C Jagadish, X Sun, and K L Teo, *Sci. Rep*. **2** (2012) 533.
21. D C Look, "*Electrical Characterization of GaAs Material and Devices*", John Wiley (1998).
22. D C Look, D C Reynolds, J R Sizelove, R L Jones, C W Litton, G Cantwell, and W C Harsch, *Solid State Commun*. **105** (1998) 339.
23. E Furno, F Bertazzi, M Goano, G Ghione, and E Belloti, *Solid State Electronics* **52** (2008)1796.
24. D L Rode, *Low-field Electron Transport, Semiconductors and Semimetals* **10** (1975) 1.
25. D A Anderson and N Aspley, *Semicond.*, *Sci. Technol*. **1** (1986) 187.
26. H Ehrenreich, *J. Phys. Chem. and Solids* **8** (1995) 130.
27. H Brooks, *Phys. Rev*. **83** (1951) 879.
28. H Tang, W Kim, A Botchkarev, G Popovici, F Hamdani, and H Morkoc, *Solid State Electronics* **42** (1998) 839
29. B Podor, *Phys. Status Solidi* **16** (1966) K167.
30. D C Look and R J Monlar, *Appl. Phys. Lett*. **70** (1997) 3377.
31. B K Ridley, *J. Phys.* C **15** (1982) 5899.
32. K Hirakawa and H Sakaki, *Phys. Rev.* B **33** (1986) 8297.
33. K Lee, M S Shur, T J Drummond, and H Morkoc, *J. Appl. Phys*. **54** (1983) 6432.
34. P K Basu and B R Nag, *Phys. Rev.* B **22** (1980) 4849.

35. J P Price, *Ann. Phys.* **133** (1981) 217.
36. P J Price and J Vac, *Sci. Technol*. **19** (1981) 599.
37. K Hess, *Appl. Phys. Lett*. **35** (1979) 484.
38. C T Sah, T H Ning, and L L Tscopp, *Surf. Sci*. **32** (1972) 561.
39. S D Sarma and F Stern, *Phys. Rev.* B **32** (1985) 8442.
40. J H Davies, "*The Physics of Low Dimensional Semiconductors*", Cambridge University Press (1998).
41. D C Look, R L Jones, J R Sizelove, N Y Garces, N C Giles, and L E Halliburton, *Phys. Status Solidi a* **195** (2003) 171.
42. F Vigue, P Vennegues, C Deparis, S Vezian, M Laugt, and J P Faurie, *J. Appl. Phys*. **90**, 10 (2001) 5115.
43. J A Davis and C Jagadish, *Laser Photon. Rev*. **3** (2008) 85.
44. N G Weimann, L F Eastma, D Doppalapudi, H M Ng, and T D Maustakus, *J. Appl. Phys*. **83** (1998) 3656.
45. T Ando, A B Fowler, and F Stren, *Rev. Mod. Phys*. **54** (1982) 437.